Journal of Materials Chemistry A

Accepted Manuscript

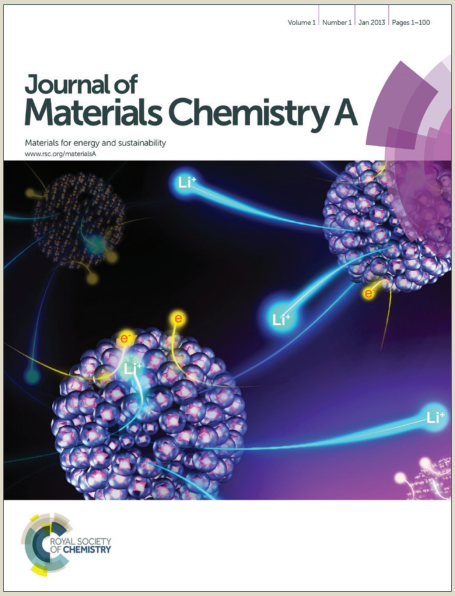

This is an *Accepted Manuscript*, which has been through the Royal Society of Chemistry peer review process and has been accepted for publication.

Accepted Manuscripts are published online shortly after acceptance, before technical editing, formatting and proof reading. Using this free service, authors can make their results available to the community, in citable form, before we publish the edited article. We will replace this *Accepted Manuscript* with the edited and formatted *Advance Article* as soon as it is available.

You can find more information about *Accepted Manuscripts* in the Information for Authors.

Please note that technical editing may introduce minor changes to the text and/or graphics, which may alter content. The journal's standard Terms & Conditions and the Ethical guidelines still apply. In no event shall the Royal Society of Chemistry be held responsible for any errors or omissions in this *Accepted Manuscript* or any consequences arising from the use of any information it contains.

ROYAL SOCIETY OF CHEMISTRY

www.rsc.org/materialsA

TABLE OF CONTENTS

Efficient oxidation of aromatic alcohols and toluene to corresponding aldehydes selectively by active surface exposed CeO_2 nanocube heterogeneous catalyst

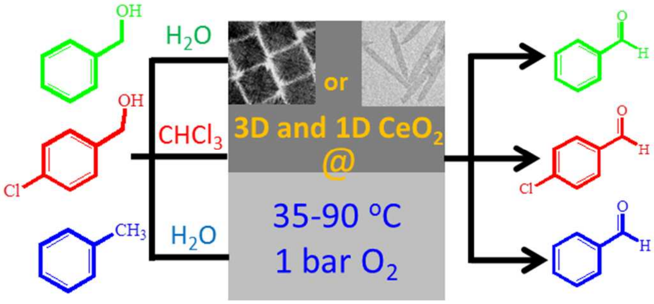

Journal of Materials Chemistry A Accepted Manuscript

(100) surface exposed CeO_2 Nanocube as Efficient Heterogeneous Catalyst in Tandem Oxidation of Benzyl Alcohol, *para*-Chlorobenzyl Alcohol and Toluene to Corresponding Aldehydes Selectively

Kalyanjyoti Deori, Chinmoy Kalita, Sasanka Deka*
Department of Chemistry, University of Delhi, North campus, Delhi-110007, India
Email: sdeka@chemistry.du.ac.in, ssdeka@gmail.com

Abstract: A new synthesis strategy has been developed to synthesize exclusively (100) surface exposed CeO_2 nanocubes (~90 nm) as efficient heterogeneous catalyst for multiple selective oxidation reactions, which are formed through three dimensional (3D) self-assembly of smaller ceria nanocrystal building blocks. For comparison of morphology effect on catalysis, 1D CeO_2 nanorods has been subjected parallelly. As-synthesized CeO_2 nanocubes acted as breakthrough catalyst in quantitative conversion of benzyl alcohol and *para*-chlorobenzyl alcohol with absolute selectivity to their respective aldehydes (>99%) under very mild reaction conditions in water at 35 ^{o}C. The same ceria nanocubes acted as efficient catalyst in the oxidation of toluene to benzaldehyde selectively. Preferred exposed (100) surfaces, the presence of higher concentration of oxygen vacancies (2.11×10^{21} cm^{-3}), small size of nanoscale building blocks and the corresponding high surface area and porosity have been reasoned for the observed high catalytic activity parameter and turn over frequency (TOF). Further characterizations on recovered catalysts after five cycles clarify the retentivity of original morphology, crystal structure and most importantly catalytic properties with no accountable activity loss, confirming the possibility of repeated use of present CeO_2 nanocubes without compromising the intrinsic qualities.

Keywords: ceria; nanocube; oxygen defect; turn over frequency; benzaldehyde.

INTRODUCTION

The high value added product like benzaldehyde and its derivative compounds are the precursors for many drugs, vitamins, fragrances, etc. and has great application in perfumery, pharmaceutical, dyestuff and agrochemical industries as well as in many organic synthesis as an important intermediates.[1,2] In the commercial practice benzaldehyde is commonly made by partial oxidation of benzyl alcohol, alkali hydrolysis of benzal chloride, liquid phase oxidation of

Journal of Materials Chemistry A Accepted Manuscript

toluene, and the carbonylation of benzene.[3-5] However the existence of chlorinated product and low selectivity towards benzaldehyde are the main concerns of these processes.[2,6] Therefore, many new routes have been introduced in recent years for the synthesis of benzaldehyde but satisfactory results were attained in only very few cases. Major drawbacks in these syntheses by such process arise from the use of base additives that often in over-stoichiometric amounts which results in carboxylate products.[7-9] Several reports described the gas phase oxidation process for the transformation of benzyl alcohol to its aldehyde, however, the uncontrolled over oxidation of products and the significant loss of carbon by forming CO_2 are the main indicated problems in these processes.[10-12] In a recent attempt, Sankar et al. resolved the issue of over oxidation and/or autoxidation of formed aldehyde to corresponding carboxylic acid in the presence of benzyl alcohol.[13] Similarly the use of toxic organic solvents and expensive metal oxidants or other stoichiometric oxidizing agent also limits the transformation process.[14,15] Therefore, liquid phase oxidation of alcohol to aldehyde by using various heterogeneous catalyst and air or molecular oxygen or mild oxidizing agent has been tasted in mild organic solvents and water to overcome such issues but with limited success.[16-18] Noble metal based catalyst such as Pt, Pd, Au, Ag and Ru have been attracted much attention now a days because of their high activity and outstanding catalytic ability.[16,19-23] Pd metal nanoparticle (NP) supported on magnesium and aluminum hydroxide has been found as efficient catalyst for the aerobic oxidation of aromatic alcohols.[19,24] Supported gold, Au-Pd alloy and bimetallic NPs catalysts also showed effective catalytic activity.[7,20,25] But noble metal based catalysts are not operationally cost effective and they cannot fulfill the global annual demand in industry. A catalyst having high surface area with larger pore size can accelerate the rate of reaction and would be highly beneficial to the oxidation process. Therefore, the development of an excellent environmentally benign, low cost, recyclable and still highly efficient heterogeneous catalyst which contain larger surface area and pore size for liquid phase aerobic oxidation of aromatic alcohol and alkane to corresponding aldehyde under mild reaction conditions is essential from both economic and environmental point of view and would constitute a breakthrough in industrial synthesis.

Being a most attractive rare-earth oxide, ceria (CeO_2) has been the subject of thorough investigations mainly because of its use as an active component in heterogeneous catalysis either in bulk or nanoparticle state.[26,27] The catalytic activity of ceria NPs is mainly associated with heightened number of oxygen defects and higher redox ability between Ce^{3+} and Ce^{4+}, which

Journal of Materials Chemistry A Accepted Manuscript

implies extremely high oxygen storage capacity of the material. The formation of non-stoichiometric oxide of general composition CeO_{2-x} through releasing or taking oxygen without decomposing or reduction in particle size is liable for oxygen vacancies within CeO_2 NPs.[28,29] This catalytically indispensable redox properties as well as surface to volume ratio of nanostructured CeO_2 are superior to their bulk counterparts and these properties can be further improved by tuning their particle size, crystallinity and most importantly the morphology.[30-32] On this basis much attention has been paid on various controlled synthesis methods to obtain monodispersed nanocrystals with interesting shapes which guarantees the exposure of different crystal planes and hence suitable surface energy.[33,34] Therefore, the fabrication of nanocrystalline CeO_2 with desired dimensionality and morphology to provide effective activity and efficiencies for catalytic purposes is still an ultimate challenge in modern material synthesis research.

In this paper, we demonstrate a simple surfactant-assisted one pot colloidal synthesis strategy for the morphology controlled synthesis of CeO_2 NPs with various interesting shapes viz., nanorods and only (100) surface exposed size controlled CeO_2 nanocubes by using two different cerium precursor. Monodispersed CeO_2 nanorods with 22-26 nm diameter and 200-210 nm length were formed when cerium acetate was used as cerium source while uniform size of 90 nm CeO_2 nanocubes were obtained by using cerium nitrate precursor. Further we have investigated the effect and ability of various shapes of CeO_2 NPs in efficiently catalyzing selective oxidation of aryl alcohols and aryl alkane into their corresponding aldehydes under very mild reaction conditions with molecular oxygen as an oxygen source and water as solvent at room temperature. Quantitative conversion of benzyl alcohol (BA) and *para*-chlorobenzyl alcohol (PCBA) with absolute selectivity to their respective aldehydes (>99%) showed a dramatic improvement in catalytic performance of cube shaped CeO_2 nanoparticles. Further this CeO_2 nanocube catalyst was found to be very effective in toluene ($PhCH_3$) oxidation as well over the nanorods. Moreover, we have shown that the CeO_2 nanoparticles catalyst can be reused for several cycles without a significant loss in activity and selectivity of the desired products in all cases.

EXPERIMENTAL

Materials. Cerium (III) acetate hydrate ($Ce(CH_3COO)_3.xH_2O$, 99.9%), cerium (III) nitrate hexahydrate ($Ce(NO_3)_3.6H_2O$, 99%), octadecene (ODE, $C_{18}H_{36}$, 90%), oleic acid (OLAC, $C_{18}H_{34}O_2$, 90%), commercial CeO_2 (99.9%) of particle size <5 μm and standard benzaldehyde,

Journal of Materials Chemistry A Accepted Manuscript

para-chlorobenzaldehyde, benzoic acid, *para*-chlorobenzoic acid samples were purchased from Sigma-Aldrich, USA. Oleylamine (OLAM, $C_{18}H_{36}N$, 70%) was purchased from Sigma-Aldrich, Netherland and 1,12-dodecanediol (DDOL, $C_{12}H_{26}O_2$, 99%) was purchased from Sigma-Aldrich, Hungary. Analytical grade of benzyl alcohol (BA, C_7H_8O, 99.9%), toluene (99.5%) and specially dried chloroform (99.9%) were purchased from Merck, India and *para*-chlorobenzyl alcohol (PCBA, $ClC_6H_4CH_2OH$, 99%) was from Merck Germany. Hydrogen peroxide solution (50% w/w H_2O_2) from Thermo Fisher Scientific, India, tertiary butyl hydrogen peroxide (TBHP, 70% in water) from Spectrochem, India, absolute ethanol (99.9%) from ChangshuYangyuan Chemical, China and acetone (99.5%) was purchased from SRL, India. All chemicals were used as received without further purification.

Synthesis of CeO_2 Nanocubes. 3-dimensional ceria nanocubes were prepared following our recent report with some additional modifications to get purely (100) surface exposed size controlled CeO_2 nanocubes.[35] In a typical synthesis procedure 1 mmol of $Ce(NO_3)_3.6H_2O$ (0.434g), 2 mL of OLAC, 2 mL of OLAM, 4 mL of ODE and 2.5 mmol of DDOL (OLAC:OLAM:DDOL ratio= 1:1:2.5) were added in a three-necked round-bottom flask (RB, 50 mL). The RB was then fitted with a condenser to a Schlenk line containing two different line viz., vacuum line and nitrogen line and placed onto a heating mental with a magnetic stirrer. The exact reaction temperature was controlled by placing a thermocouple into the reaction solution which was equipped with a programmable temperature controller. The reaction solution was at first degassed at 100 °C with vigorous magnetic stirring, and kept for 30 min at this temperature under vacuum to remove adsorbed water and oxygen, resulting in the formation of a clear solution. The temperature was then increased to 300 °C at a heating rate of approximately 15 °C min^{-1} under nitrogen atmosphere. During this reaction process under nitrogen atmosphere, after reaching around 200 °C the reaction solution suddenly became turbid and its color turned to brown suggesting the beginning of nucleation of CeO_2. After completion of 90 minutes reaction time at 300 ^oC, the heating apparatus was removed and the reaction mixture was cooled to room temperature naturally and purified by decantation and centrifugation method using acetone and ethanol. The precipitate can be re-dispersed in nonpolar solvents like toluene and hexane. After precipitation some amount of solid products were dried in oven at 40 °C overnight and kept it for further characterization and catalytic activity. The experimental yield of the synthesis was

Journal of Materials Chemistry A Accepted Manuscript

Journal of Materials Chemistry A Accepted Manuscript

determined after annealing the as-synthesized sample at 400 °C in air atmosphere to remove the surfactants and found to be 88%.

Synthesis of CeO_2 Nanorods. For the synthesis of CeO_2 nanorods a simple colloidal method was used. A solution mixture containing 1 mmol Ce(III)acetate hydrate (0.317 g), 2 mL of OLAC, 2 mL of OLAM, 4 mL of ODE and 2.5 mmol of DDOL (OLAC:OLAM:DDOL ratio= 1:1:2.5) were taken in a RB flask (50 mL). The reaction mixture was then treated in a similar way as discussed in CeO_2 nanocube synthesis procedure. During the reaction process, after completion of 30 minutes at 300 °C, the color of reaction solution was suddenly turned to pale whitish and became turbid which indicates the beginning of nucleation process. After completion of 90 minutes reaction time at 300 ^{o}C, the heating apparatus was removed and the reaction mixture was cooled to room temperature naturally and purified by decantation and centrifugation method as mentioned above. The experimental yield here was found to be 91%.

Instrumentation. Low resolution transmission electron microscopy (TEM) images, phase-contrast high-resolution TEM (HRTEM) measurements, selected area electron diffraction (SAED), dark-filed TEM imaging, high angle annular dark field (HAADF) imaging and scanning transmission electron microscopy (STEM) analyses were performed with a Philips Technai G^{2}30 aberration corrected transmission electron microscope operating at an accelerating voltage of 300 kV. Size histograms of the samples were derived from TEM images using the software Image-J. One drop of dilute ceria nanocrystal dispersion in toluene was applied onto a carbon coated Cu grid and allowing the solvent to slowly evaporate at room temperature for the TEM observation purpose. Powder X-Ray Diffraction (XRD) patterns of the as-synthesized products were collected at room temperature using a Bruker D8 Advance X- ray diffractometer system employing monochromatized Cu Kα radiation (λ = 1.54056 Å) source operating at 45 V and 40 mA. Dry powder was spread on top of a glass substrate and was then measured in reflection geometry. Fourier transform infrared spectroscopy (FT-IR) spectra (KBr disk, 4000–400 cm^{-1}) were recorded on a Perkin-Elmer FTIR 2000 spectrophotometer. Surface area of as-prepared samples was determined by Brunauer–Emmett–Teller (BET) principle and the pore parameters of the samples were determined by Barrett–Joyner–Halenda (BJH) method using 40 points BET equation with the help of Quantachrome instruments (Model: ASI-CT-11 surface area and pore size analyzer) at 77 K. A Renishaw in Via Raman spectrometer quipped with a laser having a wavelength of 514 nm was used to record Raman spectra of ceria samples at 25

^{o}C.^{1}H NMR spectra was recorded on JEOL ECX 400 NMR spectrometer operating at 400 MHz. The chemical shifts are reported in parts per million (ppm) relative to tetramethylsilane or residual solvent signal.

Catalytic Measurements. All catalytic measurements were carried out in a RB flask connected with a reflux condenser containing a magnetic stirrer in the RB. In typical reactions a mixture of 1 mmol substrate (either benzyl alcohol or *para*-chlorobenzyl alcohol or toluene), 10 mg ceria catalyst (either CeO_2 nanocube or nanorod) and 10 mL of suitable solvent (water or chloroform) was treated at a temperature range 35–90 ^{o}C and 1 bar oxygen pressure. For all substrates, molecular oxygen from oxygen cylinder was used as oxygen source. However, for getting an optimum result in the case of PCBA and toluene conversion, some milder and environmentally friendly oxidizing agents like H_2O_2 and TBHP were also used in the identical reaction conditions instead of molecular oxygen and are mentioned specifically in respective sections.

The progression of the oxidation reactions by molecular oxygen were monitored by the oxygen uptake method and GC analysis. In case of oxygen uptake method, a manometric apparatus connected to a three-neck jacketed glass reactor equipped with an impeller was used for maintaining oxygen saturation of the solution. The reactor was thermostated at required temperature by means of a circulating water bath. Oxygen consumption was measured by monitoring the decrease in volume of pure oxygen at a constant pressure (1 atm), in the manometer connected to the reactor. The initial reaction rates were calculated from the slope of the linear plots of the volume of oxygen consumption against time. Oxidation products of the catalysis reactions were analyzed by NMR and FT-IR and quantification was calculated by GC, having calibrated the method with known compounds, qualitatively and quantitatively. For GC analysis, reaction solution was centrifuged at 2500 rpm to separate out the catalyst and aliquots were then transferred to a RB flask. Water solvents were completely removed from the RB flask by using rotor vapor at 110 ^{o}C and redissolved the final product in 2 mL of chloroform. Finally 100 µL of above product solution was again diluted to 1 mL with chloroform in a 2 mL vial. The diluted solution was then run through the GC column. GC analysis was performed in a Shimadzu GC-2010 Plus instrument by using N_2 as a carrier gas and Rtx-5 column (30 m × 0.25 mm × 0.25 mm, Restek, USA). The oxidation products were identified by their retention times in comparison with authentic samples. Each peak of the GC chromatogram was integrated and the

Journal of Materials Chemistry A Accepted Manuscript

Journal of Materials Chemistry A Accepted Manuscript

actual concentration of each component was obtained from the pre-calibrated plot of peak area against concentration.

RESULTS AND DISCUSSION

Structural and Morphology Studies of CeO_2 Nanoparticles.

The morphology study of as-prepared CeO_2 nanocrystals by one pot colloidal method using cerium (III) nitrate hydrate precursor was first analyzed by TEM, HRTEM and XRD, and the results are shown in Figure 1. In our recent report we have successfully utilized CeO_2 nanocubes exposed with (200) and (220) crystal planes in quantitative *para*-xylene conversion to terephthalic acid with absolute selectivity (>99%).[35] In that three dimensional oriented attachment synthesis reaction where 60 min was the reaction time, three dimensional (3D) assembly of (100) and (110) surface exposed porous CeO_2 nanocube formed via oriented attachment of the nanocrystal building blocks by sharing {111} facets. In order to get purely (100) surface exposed CeO_2 nanocubes and diminished the exposure of less energetic (111) and (110) crystal planes completely, we have carried out the synthesis of ceria nanocube for 90 min as described in the experimental section instead of 60 min. Only one type of exposed surface i.e., most energetic (100) surface which is highly defective, contains high oxygen vacancies and hence most important in catalytic point of view is exclusively visible under the current study.[28,29,36] As shown in Figure 1a the powder XRD profile of as synthesized CeO_2 nanocube after 90 minutes of reaction time can be indexed to CeO_2 fluorite structure (space group = *Fm3m*, JCPDS card #34-0394). All characteristic XRD peaks are purely matching with bulk CeO_2 thus confirm the high purity of our as synthesized CeO_2 nanocubes. The lattice constant was calculated and found to be 5.415 Å. The average crystallite size was calculated using the Scherrer formula and found to be 6.7 nm. Further, we have investigated all XRD pattern at lesser colloidal reaction time viz., 15 minutes 30 minutes and 60 minutes. Interestingly, from the peak intensity ratio of (200)/(111) planes obtained from XRD patterns of Figure 1a and Figure 2a, we can get some useful information regarding the growth of (100) surfaces at the expense of {111} facets upon increasing the reaction time. The peak intensity ratio of (200)/(111) planes were found to be 0.27 and 0.36 for reaction time 15 minutes and 30 min respectively which were slightly higher than that of bulk intensity ratio (0.26), but when the reaction time was further increased to 90 min, the same intensity ratio was found to be unexpectedly high, i.e., 0.84 (see Figure 1a). This peak intensity ratio of (200)/(111) planes at 90 min of reaction which is almost two times larger than that of reaction carried out at 60 min provide some initial insight on the growth of only (200) planes.

It can be seen from the low magnified TEM imaging (Figure 1b) of as-synthesized CeO_2 nanoparticles that the shape of all CeO_2 nanoparticles is exclusively nanocube type with uniform size of 90 nm and purely monodispersed in nature. The average particle size measured by TEM is around thirteen to fourteen times larger than that calculated from the Scherrer equation (6.7 nm). On Z-contrast elemental mapping in the STEM mode, we have observed homogeneous distributions of Ce and O over one single cubic nanoparticle (Figure 1c-e). STEM-EDX analysis presented in Figure 1f showed stoichiometric nature of as synthesized CeO_2 nanocubes with Ce:O ratio 1:2.

Further when the sample is closely monitored under HRTEM and high magnified TEM, it was found that the cubic shaped 90 nm particles are actually made by very small CeO_2 nanoparticles of 6–7 nm size which are self-aggregated to form a big cubic particle due to the presence of various organic surfactants like oleylamine (OLAM) and dodecanediol (DDOL) and most importantly (100) surface selective surfactant oleic acid (OLAC) as described in earlier report.[35] The morphology and the structure of the final products were further examined by phase contrast HRTEM. All ceria nanocubes are composed of small nanoparticles; the foam like pores can easily be seen in Figure 1g (see Figure S2). Detailed HRTEM analysis on a single CeO_2 nanocube (Figure 1h) further revealed that after 90 min of reaction not only the uniform morphology was obtained but predominantly (200) planes were detected exclusively everywhere on the CeO_2 nanocubes. The sharp spotty pattern of (200) ring on SAED image and 2D-FFT calculation (inset of Figure 1h) also reflect the exposure of {100} facets predominantly. Furthermore, Spotty SAED pattern of as-synthesized CeO_2 nanocubes revealed the pure crystalline nature with cubic fluorite structure, where (200), (220), (311) and (400) lattice planes were clearly indexed. Aliquots from the reaction vessel at different time intervals were collected and the collected data on characterizations are compared in Figure 2. Aggregated nanoparticles containing less cubes with average size of 10-15 nm and 20-30 nm at the early reaction times of 15 and 30 min, respectively, indicate the initiation of self assembly process and can clearly be seen in TEM images (Figure 2e,f). Although 44-46 nm size nanoparticles with uniform cubic morphology were obtained after 60 minutes of reaction time, however at this moment the crystal growth was not complete (Figure 2g) and only after 90 minutes of reaction a perfect nanocube

Journal of Materials Chemistry A Accepted Manuscript

Journal of Materials Chemistry A Accepted Manuscript

with complete exposure of (200) crystal planes was obtained. Furthermore, the comparison of XRD patterns, TEM images and the corresponding SAED spotty patterns at various colloidal reaction times clearly demonstrated gradual increase of (200) ring intensity upon increasing the reaction time (Figure 2b-d). Finally a narrow size distribution was observed from particle size distribution histogram as depicted in Figure 1i over a large number of particles.

To clarify the presence of 6-7 nm nanoscale buiding blocks and to prove the extensively exposed (100) surfaces of the present ceria nanocubes, few controlled reactions have been performed. When oleic acid surfactant was not used in the identical reaction condition, only 4-6 nm size of polyhedral nanopartilces were formed with exposed (111) crystal planes. In the presence of oleic acid, at the initial reaction time small polyhedral nanocrystals building blocks were formed which exposes (111) crystal planes, however with progression of time these smaller CeO_2 nancrystal building blocks start assembling by sharing {111} facets due to the preferential adsorption of oleic acid on the (100) surfaces.[35] Hence it makes the (111) surfaces more vulnerable for growth or attachment and small CeO_2 nanocrystals act as building blocks and started assembling a 3D cubic morphology by sharing the {111} facets.

We then explored further other morphology of CeO_2 nanoparticles, to examine the effectiveness of topology, exposed surfaces and possible oxygen defects on the industrially important alcohol to aldehyde catalytic oxidation reactions. The characterization results of samples in the second synthesis in terms of TEM and powder XRD are summarized in Figure 3. A large quantity of monodispersed nanorods is clearly seen from low magnification TEM images (Figure 3a). The average diameters of the as synthesized nanorods are in the range of 22-26 nm, and the lengths in the range 200–210 nm (see histogram in ESI, Figure S1). As shown in Figure 3d (iii) the powder XRD pattern of as-synthesized CeO_2 NRs clearly indicates the low crystallinity of sample. The amorphous nature of as prepared sample was again confirmed by SAED image depicted in the inset of Figure 3a. Therefore the nanorod sample was further annealed at 400 ^oC for 3 hours and again performed XRD and TEM analysis. The morphology and size of the resultant CeO_2 nanorods remains intact after thermal treatment at 400 ^oC in air atmosphere (Figure 3b) and thus lattice fringes were observed in phase contrast HRTEM analysis. From Figure 3c distinctive set of fringes can be unambiguously identified, such as those corresponding to (111) planes of bulk *fcc*-CeO_2 ($d_{111}^{CeO2} = 0.31\ nm$) and (200) plans of CeO_2

(d_{200}^{CeO2} = 0.27 nm). The crystallinity of resultant CeO_2 nanorods can be further verified by spotty SAED pattern shown in inset (i) of Figure 1c, which reveal polycrystalline nature of annealed sample with cubic fluorite structure, where (111), (200), (220), and (311) lattice planes were clearly indexed. 2D Fast Fourier Transform (2D-FFT, inset: ii) generated from HRTEM image of panel 'c' also confirmed the presence of (111) and (200) crystal planes. The X-ray diffraction (XRD) measurements of nanorod sample after post heating treatment have been examined at 2θ ranging from 10° to 80°, for structural and phase purity studies. As shown in Figure 3d, the characteristic XRD peaks of experimental sample located at 2θ =28.54, 33.08, 47.50, 56.35, 59.09, 69.42, 76.71 and 79.08° are purely matching with bulk CeO_2 (JCPDS card #34-0394) which are corresponding to (111), (200), (220), (311), (222), (400), (331) and (420) crystal planes, respectively. All these observed peaks correspond to a face-centered cubic (*fcc*) fluorite structure of CeO_2 with space group =*Fm3m*, space group number =225, and lattice constant *a*=5.411 Å. No other crystalline by-products or other cerium oxide phases were found in the experimental pattern, confirming the high purity and crystallinity of annealed product.

At this stage question arises on the role of NO_3^- and CH_3COO^- ions of cerium salts on the selectivity towards the evolution of nanocube and nanorod morphology and particle crystallinity. Since both the synthesis procedures are identical except the presence of two different anions, it is clear that these two anions alter the nanoparticle formation mechanism in different pathways. Nitrate ion present in the Cerium (III) nitrate precursor itself acts as a strong oxidizing agent which can provide oxygen to facilitate CeO_2 nucleation. These nitrate ions can also selectively bind to (100) crystal planes of CeO_2 nucleus and hence in this case, as synthesized particles we have found is purely crystalline CeO_2 nanoparticles with cubic morphology. However, in the presence of acetate ions in cerium precursor the as synthesized product is not purely fluorite structure of CeO_2 nanoparticles and phase is amorphos in nature as shown in Figure 3d (panel iii). So, for preparing purely crystalline CeO_2 nanoparticles by using cerium(III) acetate precursor the as synthesized sample has to be air annealed at high temperature (Figure 3d, panel ii). We believe that like some other counteranions viz., Cl^-, Br^-, I^-, SO_4^{2-} etc. acetate ion has also very weak adsorption tendency towards CeO_2 surface and hence initial $Ce(OH)_3$ nucleation facilitate anisotropic growth to form nanorods due to dissolution-recrystallization equilibrium remain unaffected according to Wu et al.[37]

Journal of Materials Chemistry A Accepted Manuscript

Surface Capping, Surface Area and Oxygen Vacancy Defects of As-Synthesized CeO_2 Nanoparticles.

As discussed earlier the presence of surface selective surfactants are responsible for the formation of (100) surface exposed CeO_2 nanocubes. Figure 4a depicts FT-IR spectrum of as synthesized CeO_2 nanocubes sample which confirms the presence of various surfactants on the surface of nanocubes. The presence of oleic acid surfactants can be confirmed from the sharp absorption peak in the region 1400-1600 cm^{-1} and at 2847 and 2926 cm^{-1} due to C-O of the $-COO^{-}$ group and C-H symmetric and asymmetric stretching vibrations respectively. However the sharp IR absorption peak at 3434 cm^{-1} is attributed to N-H stretching vibration of amine groups of OLAM. In addition the broad absorption peak in the region of 400-650 cm^{-1} is due to O-CeO_2 stretching vibration. To know the exact surface area of our as synthesized porous CeO_2 nanocubes sample we have performed a detailed N_2 adsorption–desorption study from which specific surface area and porosity were measured at temperature 77 K. Before starting the measurement, sample was degassed at 150 ^{O}C for 8 h. It is clearly seen from the plot in Figure 4b that the behavior of isotherm is combination of type II and type V and hysteresis is H3 type. By using the multipoint BET equation, specific surface area of as synthesized CeO_2 nanocube sample was found to be 159 m^2/g. This higher surface area is mainly attributed to the 3D assembly of the small CeO_2 crystallites (6-7 nm). Further the pore size distribution was calculated from the Barrett-Joyner-Halenda (BJH) method and a maximum pores distribution was observed at 1.3 nm (intrinsic) of pore radius with a few more pores in the range of 3-5 nm (extrinsic, mesoporosity), although they do not evidence the presence of regularly ordered pores (inset of Figure 4b). These extrinsic pores of 3-5 nm could be explained from the observation of foam like pores in Figure 1g and under dark-field TEM imaging (Figure S2), which are actually gap between small nanocrystallite building blocks. This observation of high number of pores could be indicative towards the presence of very essential densely defects on high energy surfaces and this statement is proved in the next paragraph with the help of Raman spectroscopic analyses.

A typical Raman spectrum of as-synthesized nanocubes and nanorods sample can be seen from Figure 4c,d where a sharp Raman peak at a frequency of 462 cm^{-1} and 461 cm^{-1} was observed for symmetrical stretching mode of the Ce-O8 vibrational unit of CeO_2 nanocubes and nanorods sample, respectively.[38,39] From the Raman spectrum the concentration of oxygen

Journal of Materials Chemistry A Accepted Manuscript

vacancies at the surface of as synthesized CeO_2 NPs were evaluated by calculating the grain size of nanocrystals using the following equations:[35,38,39]

$$d_g(nm) = \frac{51.8}{\Gamma(\mathrm{cm}^{-1}) - 5} \tag{1}$$

$$L\,(nm) = \sqrt[3]{\left(\frac{\alpha}{2d_g}\right)^2 \left[\left(d_g - 2\alpha\right)^3 + 4d_g^2\alpha\right]} \tag{2}$$

$$\mathrm{N} = 3/4\pi \mathrm{L}^3 \tag{3}$$

Where 'd_g' is grain size, 'Γ' is half-width at half-maximum (HWHM) in cm^{-1}, 'L' is correlation length (average distance between two lattice defects), α is the radius of CeO_2 units (0.34 nm) determined from universal constants and N is the oxygen vacancy concentration in cm^{-3}. A very high value of oxygen vacancy concentration viz. 2.11×10^{21} cm^{-3} was obtained in the case of CeO_2 nanocubes sample compared to the value of CeO_2 nanorods sample which is 1.02×10^{21} cm^{-3}. This observed almost two times higher oxygen vacancy value on ceria nanocubes than the nanorods and in good correlation with other reported ceria NPs[38,39] made present nanocube sample more interesting and beneficial in terms of catalytic activity. This high value of oxygen vacancy could be is attributed to the small ceria nanocrystals (4-6 nm) which are self-oriented to form 90 nm size nanocubes with the exposure of highly defective (100) surfaces.

Catalytic Study.

Aerobic oxidation of benzyl alcohol, *para*-chlorobenzyl alcohol and toluene with molecular oxygen were carried out under mild reaction conditions using water and chloroform as solvents in the presence of CeO_2 nanocube (CNC) and nanorod (CNR) catalysts, respectively. A reaction mixture containing 1 mmol (108 mg) benzyl alcohol, 10 mL water and 10 mg CNC in a RB flask with a reflux condenser was treated at 35 °C and 1 bar oxygen pressure, by measuring the volume of O_2 consumption with time for preliminary investigation. As shown in Figure 5 from the slope of the linear plot we have calculated initial rate of reaction which was converted to concentration unit and found to be $r_i = 67 \times 10^{-3}$ mol $L^{-1}min^{-1}$ (Table 1, entry 1). We noticed that total 7.5 mL oxygen was consumed in 30 min of reaction, which proved a higher rate of reaction. The reaction was stopped at this time and aliquot was collected after centrifugation and

Journal of Materials Chemistry A Accepted Manuscript

tested it by GC. The similar procedure was continued for the next five batch of recyclability test and the observed initial rates are summarized in Table 1. For performing the recyclability test catalyst was recovered by centrifuging the reaction solution at 2500 rpm and then washed, dried and reused for the next cycle. It is clearly seen from Table 1 that our as-synthesized CNC catalyst can be reused for many catalytic cycles without a significant loss of activity, thus showing very efficient and heterogeneity towards benzyl alcohol oxidation process. To check why our CNC catalyst is so effective and is it because of energetic surface exposed in CNC, we had thoroughly investigated the catalysis of CNR also. As shown in Figure 5 and Table 1 (entry 6) the oxygen consumption rate was comparatively slower when CNR catalyst was used in the same reaction by replacing it with CNC. The initial rate of reaction for this sample was calculated as r_i = 26 × 10^{-3} $\text{molL}^{-1}\text{min}^{-1}$, which is about 2.5 times slower than CNC catalyst. To further characterize the kinetics of the CNC catalyzed reactions, we have calculated the turn over frequency (TOF) and activity parameter (*K*) of the catalyst using the following equations.

$$\text{TOF} = \frac{-k_{app}(min^{-1})\ x\ [50\%\ product](M)}{[CeO_2\ NP](M)} \tag{4}$$

$$\text{k}_{\text{app}} = \frac{r_1}{[reactant]} \tag{5}$$

$$\text{K} = \text{k}_{\text{app}}/\text{m} \tag{6}$$

where k_{app} is the apparent reaction rate constant and *m* is the catalyst loading. TOF is the intrinsic rate at which a catalytic cycle turn over on an active site. However in a heterogeneous catalyst system number of active site depends on various surface properties, such as surface area, oxygen defects, catalyst loading, etc. In the present case TOF is calculated based on the time required (8 min) for 50% product formation using 10 mg/10 ml (catalyst/solvent) concentration for more accurate comparison. The TOF is found to be 5.777 min^{-1} and at the same time activity parameter is found to be 67 $\text{min}^{-1}\text{g}^{-1}$. Thus CNC catalyst possesses highly active surfaces to oxidize large number of molecules of each alcohol per unit amount of catalyst in a very short time. These preliminary investigations clearly suggest the significant role of (100) exposed crystal planes and high oxygen defect concentrations of CNC in the direction of oxidation transformation. To reevaluate the effectiveness of CNC catalyst we have performed a blank reaction without adding any catalyst in the identical reaction condition. No significant consumption of oxygen was observed until 2 hours. When commercially purchased bulk CeO_2 was used as a catalyst only 8-10% benzyl alcohol conversion was confirmed by GC analysis.

Journal of Materials Chemistry A Accepted Manuscript

Journal of Materials Chemistry A Accepted Manuscript

The progress of reaction was further monitored by thin layer chromatography (TLC) and 2,4-Dinitrophenylhydrazine (DNP) test for aldehydes. The precipitate of DNP derivatives confirms the formation of aldehyde, hence the final reaction solution containing the oxidation products after removal of catalyst was then evaluated by NMR, IR and GC techniques. Quantification of obtained results viz., substrate conversion, product selectivity and product yield were calculated from GC data as follows:

$$\text{Substrate conversion (\%)} = \frac{\text{moles of converted substrate x 100}}{\text{moles of reactant in feed}} \tag{7}$$

$$\text{Product selectivity (\%)} = \frac{\text{moles of product formed x 100}}{\text{moles of reactant converted}} \tag{8}$$

$$\text{Product yield (\%)} = \frac{\text{substrate conversion (\%)} \times \text{product selectivity (\%)}}{100} \tag{9}$$

In the presence of 10 mg CNC catalyst BA showed quantitative conversion (99.95%) towards benzaldehyde selectively (>99%) under the reaction condition of 10 mL water and 1 mmol BA under continuous flow of molecular oxygen at 35 ^{o}C in 30 min (Table 2, entry 1). FT-IR spectrum, GC chromatogram and NMR spectrum of produced benzaldehyde sample after catalysis reaction are depicted in Figure S3-S5. As shown in Figure 6 this surprising activity of CNC could be continuing for many next batches of catalytic cycles without significant loss of activity. In the next batches of catalytic cycles by using the recovered catalyst, identical reaction condition was again set up by adding fresh benzyl alcohol (1 mmol) and water (10 mL). At the end of the reaction, reaction mixture was collected and tasted by TLC in 10% ethylacetate and hexane mixture and finally analyzed by GC. The results as shown in Figure 6 suggest that loss in activity of the catalyst after 5th cycles, in terms of substrate conversion and benzaldehyde yield was only 2.64% and 2.50%, respectively. To check the stability of the crystal structure, morphology and surface capping agents of recovered CNC catalyst over the period of 5 catalytic cycles XRD, TEM and FT-IR analysis have been carried out again on the recovered samples and the results are shown in Figure 7. It could be clearly ascertain from Figure 7a that the CeO_2 nanocubes retained the original fluorite structure as shown earlier in Figure 1a even after 5 repeated catalytic cycles. Similar retention behavior of particle morphology and surface capping is observed by comparing Figure 7b with Figure 1b,g and Figure 7c with Figure 4a. Hence, it is now confirmed that, our as-synthesized ceria nanocubes could be used for several times as efficient and highly active catalyst in selective production of benzaldehyde without compromising the quality of the particles. Similar characterization measurements have been performed on recovered ceria nanorod catalysts after completion of five cycles of catalytic reactions. XRD and TEM analyses (figure not shown) showed the retention of fluorite crystal structure and nanorod morphology with identical dimensions in comparison to as-synthesized nanorods (Figure 3).

We believe that the presence of only one type of highly energetic facets {100} and larger pores in CNC catalyst are two important reasons for its effectiveness. Moreover, the presence of higher oxygen defect concentrations on the surface of CNC catalyst is another major reason of showing better catalytic activity over CNR catalyst. When CNR was used instead of CNC at the identical reaction condition for BA oxidation, although we got complete selectivity towards benzaldehyde, the BA conversion was low which only 66.7% is even after 2 hours of reaction time compared to 99.9% conversion after 30 minutes in the later case (Figure 8 and Table 2, entry 2). We have then rechecked our catalysts again in the chloro- derivative of benzyl alcohol i.e. *para*-chlorobenzyl alcohol oxidation process. A similar trend was observed where CNC catalyst showed better activity than CNR. We found that PCBA oxidation was not effective in water as former is not soluble in water and hence at an identical reaction condition contain 10 mL chloroform ($CHCl_3$) was used as solvent in the place of water. Under molecular oxygen environment PCBA showed effectively 62% conversion with exclusively produced aldehyde selectively >99% (Table 2, entry 3) which is about 37.6% lower than BA oxidation in terms of conversion and selectivity (Figure 8). The yield was further improved by introducing H_2O_2 a milder environmentally friendly oxidizing agent in place of O_2 in the reaction mixture. PCBA conversion was drastically increased to ~92% (Table 2, entry 4) under this condition even at lesser reaction time (1h) with absolute selectivity (Figure 8, and for GC chromatogram see Figure S6). We had further tried to improve the conversion of PCBA by increasing the reaction time from 1 hour to 2 hour and then 4 hour but in these cases instead getting an improved yield we had to face the over-oxidation problem and the formation of corresponding carboxylic acids (Table 2, entry 5 & 6). When comparatively strong oxidizing agent such as TBHP was used, just in 1 h of catalysis process, PCBA was completely converted to its corresponding acid product (Table 2, entry 7). However, as expected 10 mg of CNR catalyst gave only 50% conversion (Table 2, entry 8 and Figure 8). To study the recyclability test over PCBA oxidation the optimum condition was then taken into consideration (Table 2, entry 4). As shown in Figure 9b the CNC

Journal of Materials Chemistry A Accepted Manuscript

catalyst retained its activity in the 5th catalytic cycle after losing just 4-5% its original activity on the basis of conversion and yield.

Further the oxidation of toluene was also investigated by using similar catalysis method, although the catalysis via oxidation of C–H bonds in the methyl group to its oxygenated products is a challenging task under a mild reaction condition. Commercially the oxidation of toluene is done with air and diluted with nitrogen (to prevent complete oxidation) at 500 ^oC in the presence of oxides of Mn, Mo or Zr as catalyst. Normally, this transformation requires harsh reaction condition like excess temperature or pressure and also need specialized equipment. Even after using of designated equipments, the selectivities to the corresponding aldehyde products are always very less and not impressive.[40] Thus there is need to improve the quality of catalyst rather than using expensive technologies in context of selective catalytic oxidation of inactive hydrocarbons to industrially important oxygenated derivatives. We have at first tried to carry out the oxidation of toluene under molecular oxygen and similar reaction environment in 10 mL water as solvent with 1 mmol toluene and 20 mg CNC catalyst. The reaction was performed at 90 ^oC for 12 h by measuring the volume of oxygen consumption. The initial rate of reaction calculated from volume of oxygen consumption vs time plot was found to be $r_i = 17 \times 10^{-3}$ $molL^{-1}min^{-1}$ which is about 4 times slower than BA oxidation and 2 times slower to PCBA oxidation. From the activity comparison plot depicted in Figure 9a showed 44.2% toluene conversion with benzaldehyde selectivity >99% which clearly shows excellent activity of CNC catalyst under mild reaction conditions compared to many other recent reports (see Figure S7 for GC analysis).[41,42] Our result at this condition is far better and seems to be exceptional than all reports till now as per our knowledge. Introduction of H_2O_2 in water and TBHP in chloroform however improved the conversion at even lower temperature and shorter time (Table 2, entry 10 & 11) but formation of over-oxidation product at this stage was the topic of concerned. Therefore, we have optimized a condition varying the catalyst amount, reaction temperature, time etc. and found as depicted in Table 2, entry 12 that a maximum of about 56% toluene conversion could be achieved with complete selectivity toward its aldehyde product by using TBHP as oxidizing agent in chloroform at 35 ^oC in 2 hours. The recyclability test performed for this reaction showed great retention of CNC's activity until 5th consecutive catalytic cycle as shown in Figure 9c. High selectivity was observed in the case of CNR catalyst also but yield was 34.2% under the above reaction conditions. Hence after evaluating all catalysis study we can

Journal of Materials Chemistry A Accepted Manuscript

Journal of Materials Chemistry A Accepted Manuscript

conclude that our as-synthesized CeO_2 porous nanocubes exposing only (100) crystal planes showed far improved catalytic activity than CeO_2 nanorods sample and the activity order is BA > PCBA > Toluene for both CNC and CNR catalyst. It has been shown theoretically as well as experimentally that the dipolar nature of (100) crystal planes of CeO_2 nanoparticles are less stable and hence highly reactive than either the (111) or the (110) surfaces, which are not associated with a perpendicular dipole.[36,43] The one kind of highly energetic surface (100) present in CNC catalyst implies highest oxygen storage capacity and consequently more important in terms of catalytic properties of the system. Although it is not a confirmative point that {100} facet is always active in any kind of catalytic reaction, for example {110} facet has also been found to be most effective for CO oxidation reaction by researchers however in our catalytic experiments we have observed {100} facet as most effective for aryl alcohol and aryl alkane oxidation reaction. As mentioned about the activity of CeO_2 nanorod catalyst, we had performed similar catalysis experiment for all substrate by using a solvothermally synthesized CeO_2 nanopolyhedra catalyst exposing (111) and (100) surfaces[44] (not mentioned in this manuscript), but the conversion and selectivity towards desired aldehyde product was found to be lowest among all catalysts in all cases.

On the basis of observed extensively exposed (100) surfaces and the corresponding high oxygen vacancies where maximum number of oxygen can be adsorbed, a schematic representation is derived (Figure 10) to show the possible dehydrogenation (oxidation) reactions on the surface of the ceria nanocubes. Conversion mechanisms of benzyl alcohol[16-18,21] and toluene[45-47] to their respective aldehyde products are well established in literature, hence in this section we are showing how those reactions take place on the present ceria surface effectively. A (100) surface of CeO_2 (corresponding to 200 *hkl* plane) is shown in part ‘a’ of the schematic, which are capped with oleic acid surfactant molecules. In the part ‘b’ of the schematic one unit of CeO_2 lattice is shown where surface oxygen atoms are missing, with respect to the observation from oxygen vacancy calculations. Since HRTEM analyses proved the presence of only high energy (100) surfaces and Raman spectroscopic studies proved the high magnitude of oxygen vacancies on these surfaces, hence all the oxidation reactions could be predicted to take place on these vacancy sites effectively as shown in Figure 10. The O–H bond of alcohol breaks upon the adsorption on surface defect sites resulting in the adsorbed alkoxide species and finally the adsorbed alkoxide will be converted to aldehyde due to supplied oxygen source. On the other hand, a free radical mechanism as suggested in literature[46,47] for toluene oxidation can be predicted in the present case also, however more efficiently due to the presence of high oxygen vacancies and (100) surfaces in CeO_2 nanocubes since the intrinsic reducibility of ceria and the formation of oxygen vacancies upon spontaneous reduction of Ce^{4+} to Ce^{3+} become critical.[48,49] Since the long chain tail of oleic acid (surfactant) is hydrophobic and benzyl alcohol substrate is partially polar in nature, at first instant it can be assumed that the reaction mechanism presented in Figure 10 may not be favorable. For the creditability of the presented mechanism, we performed few additional studies. (i) FT-IR spectroscopic measurement has been carried out on the catalyst sample after the 5th cycle. It evidenced the presence of same oleic acid surfactant and also the survival of organic surfactant at our reaction condition for the benzyl alcohol oxidation. (ii) The importance of the long tail hydrophobic end of oleic acid in the proposed mechanism has been secondly ascertained by an annealing study of the as-synthesized ceria nanocubes at 400 ^{o}C for 3 h in air atmosphere and the consequent catalytic reactions. Under comparable reaction conditions, surfactant removed annealed CeO_2 catalyst showed trace amount of benzyl alcohol, *para*-chlorobenzyl alcohol and toluene conversion with very low selectivity in corresponding aldehydes. (iii) A new batch of CeO_2 NPs has been synthesized under the similar reaction condition as mentioned in experimental section however without the addition of oleic acid (see Figure S8 for TEM image). We do not see the formation of any cubic morphology under this condition and when these particles were used as oxidation catalyst, very low conversion and selectivity were observed. These results suggest that adsorbed oleic acid surfactant and their long tail hydrophobic end played an important role by forming channels which direct the substrate molecules towards the surface of ceria through diffusion.[41]

Conclusions.

We demonstrated a simple synthesis strategy for the synthesis of only {100} facet exposed 3-dimensionally self-assembled monodispersed CeO_2 nanocube (90nm) as a breakthrough catalyst for the oxidation of aryl alcohol or aryl alkane to their respective aldehydes either in primarily green condition or in mild conditions. Furthermore, we have demonstrated the synthesis of 1D ceria nanorods and utilized them as efficient catalyst for the above purpose as well. Apart from high energetic (100) surfaces, the presence of high number of oxygen vacancies on the nanocube samples and the presence of tightly bound surfactants are found to principal reason for the observed excellent catalytic conversions over nanorod samples.

Journal of Materials Chemistry A Accepted Manuscript

Benzyl alcohol was converted selectively to commodity chemical benzaldehyde in water solvent by molecular oxygen in the presence of CeO_2 nanocubes. *para*-chlorobenzyl alcohol and toluene was also oxidized to respective aldehydes in the similar condition, however conversion efficiency and selectivity was increased by manipulating reaction conditions slightly. Finally in all cases both the amount conversion and selectivity from the substrate to the respective product are very high in the green or milder conditions, whereas, other commercial practice or reports are on very less amount of conversion and selectivity even under the use of harsh reaction conditions.

Acknowledgments. K.D. is grateful to UGC, India for research fellowship. S.D. thanks DST, India (Grant SR/S1/IC-27/2011) and University of Delhi for financial support (Grant. DRCH/R&D/2013-2014/4155). We thank Dr. S. Singh and Mr. P. Kumar for the help with GC analyses, and USIC-DU and SAIF-AIIMS for characterization facilities.

Electronic supplementary information (ESI) available: Particle size distribution histogram (Figure S1), Dark-field TEM image (Figure S2), FT-IR spectrum of as prepared benzaldehyde (Figure S3), GC chromatograph (Figure S4) and NMR spectrum (Figure S5) of the reaction products obtained from benzyl alcohol oxidation, GC chromatograph of the reaction product obtained from *para*-chlorobenzyl alcohol (Figure S6) and from toluene (Figure S7), and TEM image (Figure S8).

References:

1. S. Mandal, K. K. Bando, C. Santra, S. Maity, O. O. James, D. Mehta and B. Chowdhury, *Applied Catalysis A: General*, 2013, **452**, 94–104.
2. M. Xue, J. Yu, H. Chen and J. Shen, *Catal.Lett.*, 2009, **128**, 373–378.
3. G. W. Zhan, Y. L. Hong, F. F. Lu, A. R. Ibrahim, M. M. Du, D. H. Sun, J. L. Huang, Q. B. Li and J. Li, *J. Mol. Catal. A: Chem.*, 2013, **366**, 215–221.
4. Y. Y. Yu, B. Lu, X. G. Wang, J. X. Zhao, X. Z. Wang and Q. H. Cai, *Chem. Eng. J.*, 2010, **162**, 738–742.
5. C. Wiener and A. O. Pittet, *US Patent US 4617419 A*, 1986.
6. M. Kantham, P. Sreekanth, K. Rao, T. Kumar, B. C. Rao and B. Choudary, *US patent US20030187304 A1*, 2003.

Journal of Materials Chemistry A Accepted Manuscript

7. W. Cui, Q. Xiao, S. Sarina, W. Ao, M. Xie, H. Zhu and Z. Bao, *Catalysis Today*, 2014, **235**, 152–159.
8. G. J. Hutchings, *Chem. Commun.*, 2008, 1148–1164.
9. T. Mallat and A. Baiker, *Chem. Rev.*, 2004, **104**, 3037–3058.
10. T. L. Stuchinskaya and I. V. Kozhevnikov, *Catal.Commun.*, 2003, **4**, 417–422.
11. N. Lingaiah, K. M. Reddy, N. S. Babu, K. N. Rao, I. Suryanarayana and P. S. S. Prasad, *Catal.Commun.*, 2006, **7**, 245–250.
12. V. R. Choudhary, D. K. Dumbre, V. S. Narkhede and S. K. Jana, *Catal.Lett.*, 2003, **86**, 229–233.
13. M. Sankar, E. Nowicka, E. Carter, D. M. Murphy, D. W. Knight, D. Bethell and G. J. Hutchings, *Nature Commun.*, 2014, DOI: 10.1038/ncomms4332.
14. A. Dijksman, A. Marion-Gonzalez, A. M. Payeras, I. W. C. E. Arends and R. A. Sheldon, *J. Am. Chem. Soc.*, 2001, **123**, 6826–6833.
15. R. Liu, X. Liang, C. Dong and X. Hu, *J. Am. Chem. Soc.*, 2004, **126**, 4112–4113.
16. G.-J. Brink, I. W. C. E. Arends and R. A. Sheldon, *Science*, 2000, **287**, 1636–1639.
17. F.-Z. Su, Y.-M. Liu, L.-C. Wang, Y. Cao, H.-Y. He and K.-N. Fan, *Angew. Chem.*, 2008, **120**, 340–343.
18. G. Chen, Y. Zhou, Z. Long, X. Wang, J. Li and J. Wang, *ACS Appl. Mater. Interfaces*, 2014, **6**, 4438−4446.
19. M. S. Kwon, N. Kim, C. M. Park, J. S. Lee, K. Y. Kang and J. Park, *Org. Lett.*, 2005, **7**, 1077–1079.
20. H. Liu, Y. Liu, Y. Li, Z. Tang and H. Jiang, *J. Phys. Chem. C*, 2010, **114**, 13362–13369.
21. C. M. Zhou, Y. T. Chen, Z. Guo, X. Wang and Y. H. Yang, *Chem. Commun.*, 2011, **47**, 7473–7475.
22. Y. Shiraishi, H. Sakamoto, Y. Sugano, S. Ichikawa and T. Hirai, *ACS Nano*, 2013, **7**, 9287-9297.
23. B. Li, T. Gu, T. Ming, J. Wang, P. Wang, J. Wang and J. C. Yu, *ACS Nano*, 2014, **8**, 8152–8162.
24. U. R. Pillai and E. Sahle-Demessie, *Green Chem.*, 2004, **6**, 161-165.
25. S. Marx and A. Baiker, *J. Phys. Chem. C*, 2009, **113**, 6191–6201.
26. D. Zhang, X. Du, L. Shia and R. Gao, *Dalton Trans.*, 2012, **41**, 14455–14475.
27. M. Honda, S. Sonehara, H. Yasuda, Y. Nakagawaand and K. Tomishige, *Green Chem.*, 2011, **13**, 3406−3413.
28. F. Esch, S. Fabris, L. Zhou, T. Montini, C. Africh, P. Fornasiero, G. Comelli and R. Rosei, *Science*, 2005, **309**, 752−755.
29. C. T. Campbell and C. H. F. Peden, *Science*, 2005, **309**, 713−714.
30. X. Xie, Y. Li, Z.-Q. Liu, M. Haruta and W. Shen, *Nature*, 2009, **458**, 746−749.

Journal of Materials Chemistry A Accepted Manuscript

31. X. Mou, B. Zhang, Y. Li, L. Yao, X. Wei, D. S. Su and W. Shen, *Angew. Chem. Int. Edit.*, 2012, **51**, 2989−2993.
32. K. Zhou and Y. Li, *Angew. Chem. Int. Edit.*, 2012, **51**, 602−613.
33. X. D. Zhou, W. Huebner and H. U. Anderson, *Chem. Mater.*, 2003, **15**, 378−382.
34. H. X. Mai, L. D. Sun, Y. W. Zhang, R. Si, W. Feng, H. P. Zhang, H. C. Liu and C. H. Yan, *J. Phys. Chem. B*, 2005, **109**, 24380−24385.
35. K. Deori, D. Gupta, B. Saha and S. Deka, *ACS Catal.*, 2014, **4**, 3169−3179.
36. S. Yang and L. Gao, *J. Am. Chem. Soc.*, 2006, **128**, 9330−9331.
37. Q. Wu, F. Zhang, P. Xiao, H. Tao, X. Wang and Z. Hu, *J. Phys. Chem. C*, 2008, **112**, 17076–17080.
38. P. Trogadas, J. Parrondo and V. Ramani, *ACS Appl. Mater.Interfaces*, 2012, **4**, 5098−5102.
39. I. Kosacki, T. Suzuki, H. U. Anderson and P. Colomban, *Solid State Ionics*, 2002, **149**, 99−105.
40. Z. Sun, G. Li, Y. Zhang, H.-O. Liu and X. Gao, *Catalysis Communications*, 2015, **59**, 92–96.
41. J. Lv, Y. Shen, L. Peng, X. Guo and W. Ding, *Chem. Commun.*, 2010, **46**, 5909–5911.
42. K. T. V. Rao, P. S. N. Rao, P. Nagaraju, P. S. S. Prasad and N. Lingaiah, *Journal of Molecular Catalysis A: Chemical*, 2009, **303**, 84–89.
43. D. C. Sayle, S. A. Maicaneanu and G. W. Watson, *J. Am. Chem. Soc.*, 2002, **124**, 11429-11439.
44. K. Deori, D. Gupta, B. Saha, S. K. Awasthi and S. Deka, *J. Mater. Chem. A*, 2013, **1**, 7091–7099.
45. C. O. Baltaretu, E. I. Lichtman, A. B. Hadler and M. J. Elrod, *J. Phys. Chem. A*, 2009, **113**, 221–230.
46. S. Devika, B. Sundaravel, M. Palanichamy and V. Murugesan, *J. Nanosci. Nanotechnol.*, 2014, **14**, 3187–3192.
47. W. F. L. M. Hoeben, F. J. C. M. Beckers, A. J. M. Pemen, E. J. M. Heesch and W. L. Kling, *J. Phys. D: Appl. Phys.*, 2012, **45**, 055202.
48. S. Tsunekawa, K. Ishikawa, Z. Q. Li, Y. Kawazoe and A. Kasuya, *Phys. Rev. Lett.*, 2000, **85**, 3440–3443.
49. X. Liu, K. Zhou, L. Wang, B. Wang and Y. Li, *J. Am. Chem. Soc.*, 2009, **131**, 3140-3141.

Journal of Materials Chemistry A Accepted Manuscript

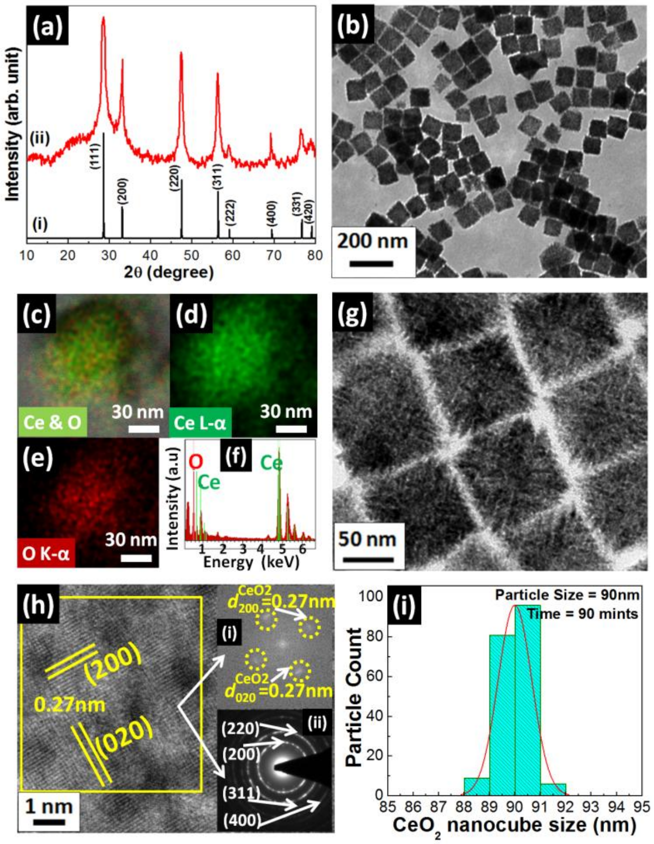

Figure 1. (a) Experimental XRD pattern of the as synthesized CeO_2 nanocubes with bulk XRD pattern of cubic fluorite CeO_2, (b) low magnified bright-field TEM image, (c) TEM elemental mapping showing both elements in a single particle, (d,e) Ce and O elemental maps from the same particle obtained by filtering the Ce L edge and O K edge, respectively, (f) TEM-EDX pattern, (g) high magnified TEM image of as synthesized CeO_2 nanocubes, (h) HRTEM image showing lattice fringes corresponding to only (200) planes seen along $\langle 004 \rangle$ zone axis, (inset i: corresponding calculated 2D-FFT pattern, inset ii: SAED pattern) and (i) particle size distribution histogram.

Journal of Materials Chemistry A Accepted Manuscript

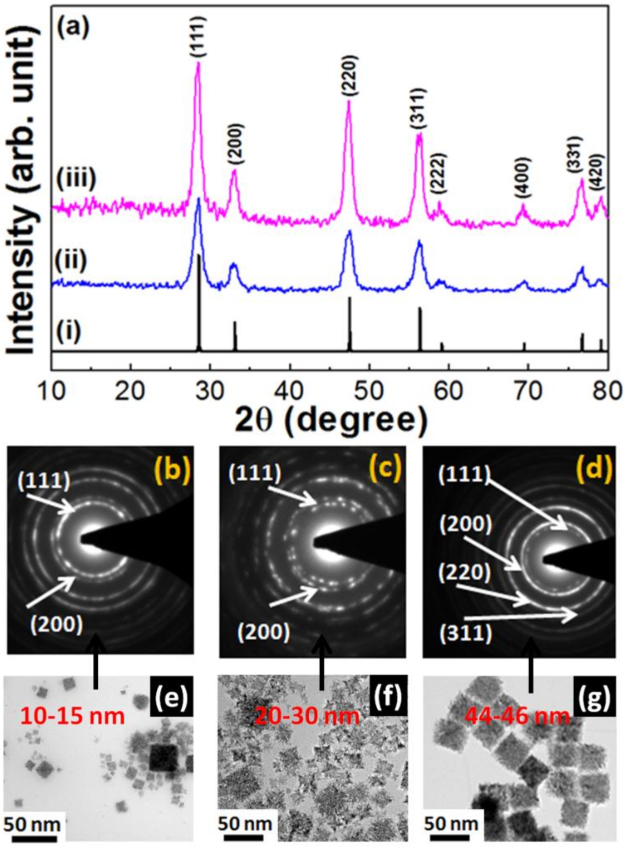

Figure 2. (a) Powder XRD pattern of the as-synthesized sample for (ii) 15 min and (iii) 30 min of reaction time and (i) of simulated bulk fluorite CeO_2. TEM images and corresponding SAED patterns from the colloidal synthesis reaction at reaction time (b,e) 15 min, (c,f) 30 min and (d,g) 60 min.

Journal of Materials Chemistry A Accepted Manuscript

Journal of Materials Chemistry A Accepted Manuscript

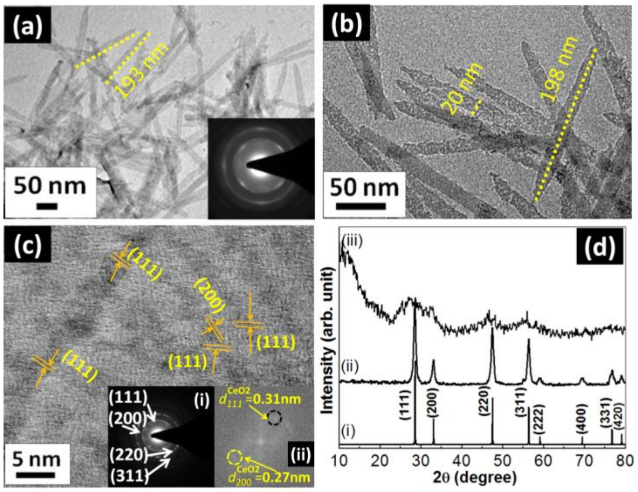

Figure 3. Low magnification TEM image of (a) colloidally synthesized CeO_2 nanorods, inset: corresponding SAED pattern and (b) CeO_2 nanorods after annealing at 400 ^{o}C for 3 hours, (c) HRTEM image of some nanorods showing lattice fringes after annealing (inset i: SAED pattern, inset ii: 2D-FFT pattern). (d) Powder XRD pattern of bulk fluorite CeO_2, JCPDS card #34-0394 (i), annealed sample (ii), and as-synthesized sample (iii).

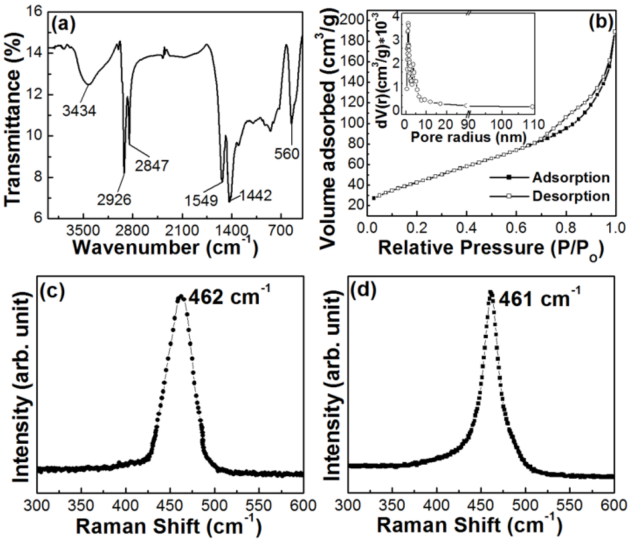

Figure 4. (a) FT-IR spectrum of as-synthesized CeO_2 nanocubes. (b) N_2 adsorption–desorption isotherm of CeO_2 nanocubes at 77 K. Inset: Pore volume distribution vs. pore radius of CeO_2 nanocubes. Raman spectrum of CeO_2 nanocube (c) and (d) CeO_2 nanorod sample at 25 ^{o}C.

Journal of Materials Chemistry A Accepted Manuscript

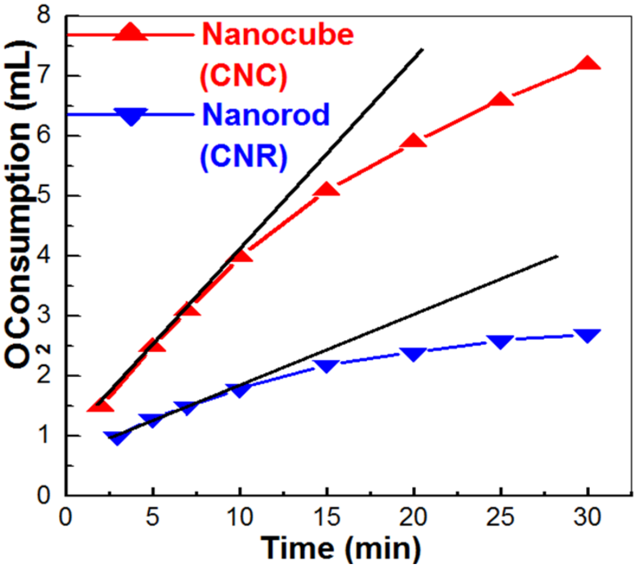

Figure 5. A plot of volume of O_2 consumption with respect to catalytic reaction time during oxidation of benzyl alcohol with 10 mg CNC and CNR catalyst, respectively at 35 °C and 1 bar oxygen.

Journal of Materials Chemistry A Accepted Manuscript

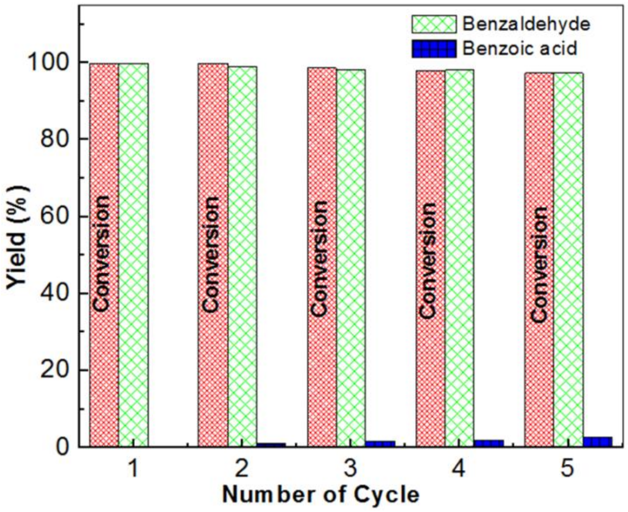

Figure 6. Recyclability study of CNC catalyst for benzyl alcohol oxidation in water at 35 °C and under molecular oxygen atmosphere.

Journal of Materials Chemistry A Accepted Manuscript

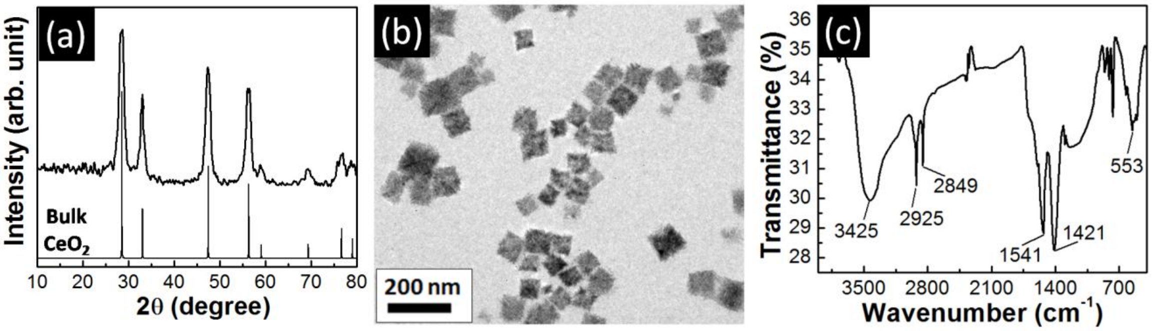

Figure 7. (a) XRD pattern, (b) TEM micrograph and (c) FT-IR spectrum of recovered CNC catalyst after 5th consecutive catalytic cycles.

Journal of Materials Chemistry A Accepted Manuscript

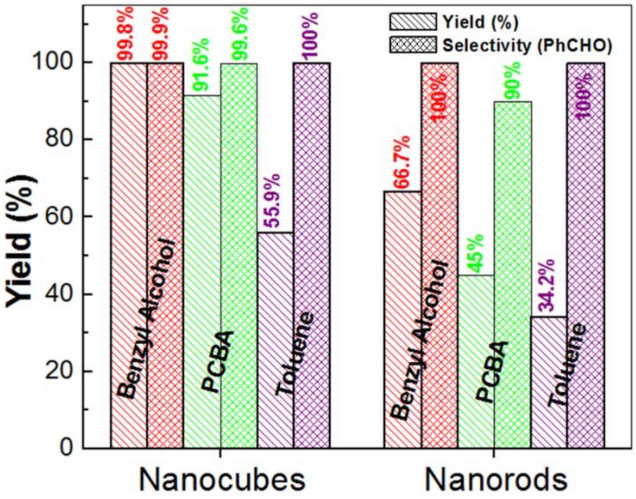

Figure 8. Comparison of CNC and CNR catalyst in terms of activity towards substrate conversion and yield of corresponding aldehydes at the best optimum reaction condition.

Journal of Materials Chemistry A Accepted Manuscript

Journal of Materials Chemistry A Accepted Manuscript

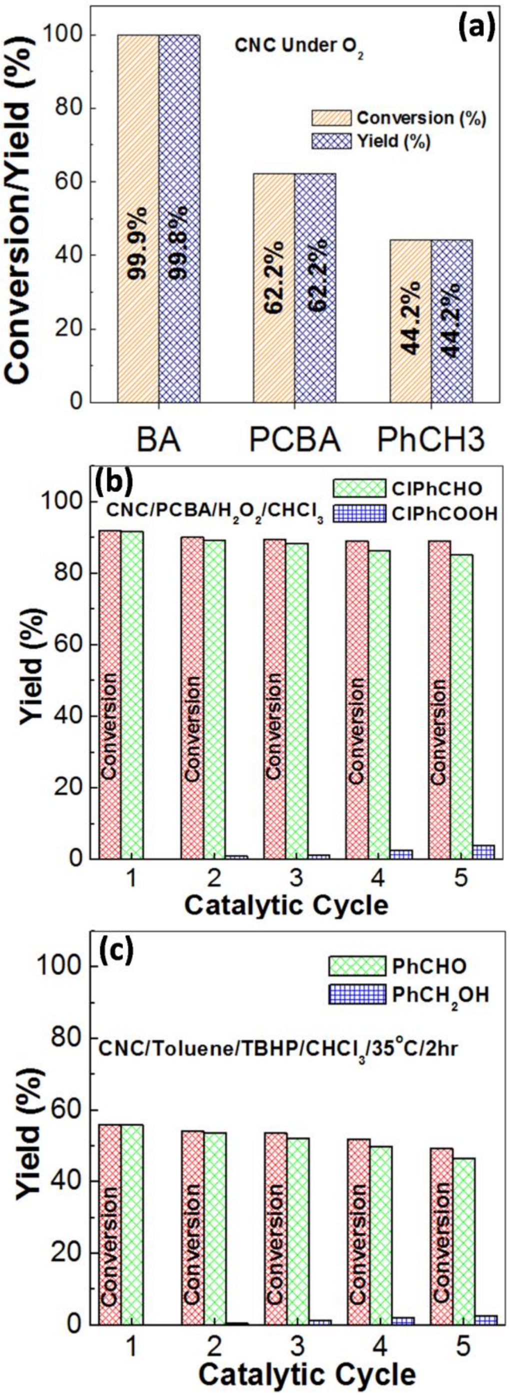

Figure 9. (a) Activity comparison of CNC catalyst in BA, PCBA and toluene oxidation process under O_2 environment, (b) Recyclability study of CNC catalyst for PCBA oxidation with H_2O_2 in chloroform at 35 °C, 1h and (c) Recyclability test for toluene oxidation with TBHP in chloroform at 35 °C by using CNC catalyst.

Journal of Materials Chemistry A Accepted Manuscript

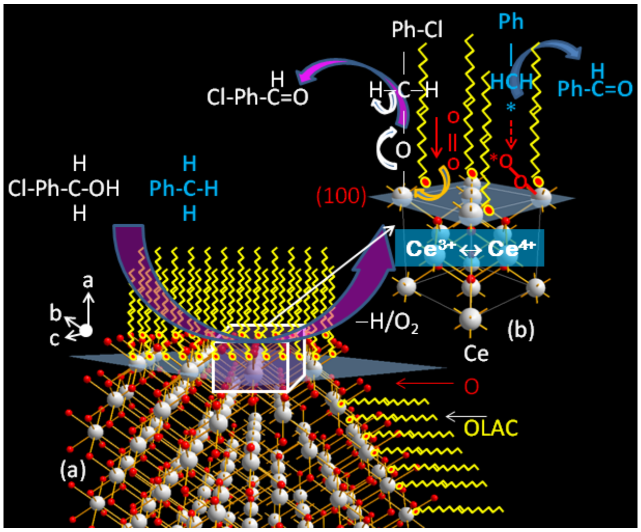

Figure 10. A mechanistic view of the possible reaction mechanism of the oxidation process of *para*-chlorobenzyl alcohol/toluene to corresponding benzaldehyde with oxygen by oleic acid enveloped ceria nanocubes.

Journal of Materials Chemistry A Accepted Manuscript

Table 1. Initial reaction rates for the CeO_2 nanocube catalyzed oxidation of benzyl alcohol after various catalytic cycles (1 mmol benzyl alcohol, 10 mL water and 10 mg catalyst).

Entry No.	Catalyst (mg)	T (°C)	$r_i \times 10^{-3}$(mol L^{-1} min^{-1})
1 (1st cycle)	10	35	67
2 (2nd cycle)	10	35	65
3 (3rd cycle	10	35	64
4 (4thcycle)	10	35	64
5(5thcycle)	10	35	62
6 (nanorod)	10	35	26

Table 2. Product distribution (conversion and selectivity^{a}) after various catalytic oxidation reactions with CNC and CNR catalyst at variable reaction conditions.

Entry No.	Starting Material	Catalyst	Oxidizing agent	Solvent	temp./time	Conversion (%)	-CHO^{a}(%)	-OH^{a} (%)	-COOH^{a}(%)
1	**BA**	**CNC**	**O_2**	**Water**	**35 °C/30m**	**99.95**	**99.86**	—	—
2	BA	CNR	O_2	Water	**35 °C**/2h	66.68	100	—	—
3	**PCBA**	**CNC**	**O_2**	**$CHCl_3$**	**35 °C/2h**	**62.18**	**100**	—	—
4	**PCBA**	**CNC**	**H_2O_2**	**$CHCl_3$**	**35 °C/1h**	**91.97**	**99.60**	—	—
5	PCBA	CNC	H_2O_2	$CHCl_3$	**35 °C**/2h	94.61	73.18	—	19.80
6	PCBA	CNC	H_2O_2	$CHCl_3$	**35 °C**/4h	96	40	—	60
7	PCBA	CNC	TBHP	$CHCl_3$	**35 °C**/1h	100	—	—	100
8	PCBA	CNR	H_2O_2	$CHCl_3$	**35 °C**/2h	50	90	—	5
9	**$PhCH_3$**	**CNC**	**O_2**	**Water**	**90°C/12h**	**44.19**	**100**	—	—
10	$PhCH_3$	CNC	H_2O_2	Water	60°C/4h	57.95	83.47	—	16.50
11	$PhCH_3$	CNC	TBHP	$CHCl_3$	35°C/4h	59.54	77	0.05	22.80
12	**$PhCH_3$**	**CNC**	**TBHP**	**$CHCl_3$**	**35°C/2h**	**55.87**	**100**	—	—
13	$PhCH_3$	CNR	TBHP	$CHCl_3$	35°C/2h	34.19	100	—	—

Journal of Materials Chemistry A Accepted Manuscript